All-terrain droplet actuation†

Mohamed Abdelgawad,[a] Sergio L. S. Freire,[b] Hao Yang[b] and Aaron R. Wheeler*[b,c,d]

Received 28th January 2008, Accepted 12th March 2008
First published as an Advance Article on the web 2nd April 2008
DOI: 10.1039/b801516c

Digital microfluidics has become a popular tool for biochemical and biomedical applications. However, its current format is restricted to actuation of droplets on a single plane. Here, we introduce a new method for fluid handling on flexible devices, which we have termed all-terrain droplet actuation (ATDA). We show that ATDA can be used to manipulate droplets across a wide range of geometries, including inclined, declined, vertical, twisted, and upside-down architectures. These new geometries enable flexible, straightforward integration of distinct physicochemical environments on monolithic devices. To illustrate this capacity, we developed temperature- and oxygen-sensitive colorimetric sensors, as well as an automated method for selective enrichment of DNA from a heterogeneous mixture. We anticipate that ATDA will be a useful new tool in the growing trend toward laboratory miniaturization.

Introduction

Digital microfluidics is a micro-scale fluid handling technique that enables manipulation of discrete droplets on an array of electrodes by means of electrowetting[1,2] or dielectrophoresis,[3,4] and has recently emerged as a useful tool in biochemical applications.[5–12] Using this technique, droplets can be manipulated through multiple, reconfigurable paths defined by the electrode actuation sequence, and, unlike microchannel devices, there is no sample wasted in creating small plugs for analysis. In addition, in digital microfluidics, each droplet is isolated from its surroundings rather than being embedded in a stream of fluid—an efficient method of forming a microreactor in which there is no possibility that products will diffuse away. However, in its standard implementation, digital microfluidics is restricted to a single horizontal plane which limits device capacity and complicates the integration of heterogeneous physicochemical environments on the same device.

In contrast to digital microfluidics, conventional channel-based labs-on-a-chip are moving towards three-dimensional configurations, formed by stacking multiple layers on top of each other.[13–17] Such devices allow for the formation of complex geometries (*e.g.*, knots and vertical actuators), and more importantly, have the advantage of much higher volumetric capacity for a given two-dimensional footprint. While there have recently been preliminary efforts towards implementing digital microfluidics on non-planar substrates, these studies have been limited by requirements of aligning a homogeneous gap between two closely spaced plates[18] and/or droplet actuation is restricted to vertical jumps between two platforms facing each other.[19]

Here, we introduce a new method for digital microfluidic transport on non-planar devices, which we have termed all-terrain droplet actuation (ATDA). In ATDA, a thin, flexible substrate is bent to form one of a wide variety of device shapes, which enables straightforward integration of distinct physicochemical environments on a monolithic platform. As has been shown for other applications,[20,21] such substrates are advantageous because of their flexibility and the efficient heat transfer through the thin material. To illustrate the advantages of the new digital microfluidic format, we developed temperature- and oxygen-sensitive colorimetric sensors, as well as an automated method for selective enrichment of DNA from a heterogeneous mixture.

Results and discussion

All-terrain droplet actuation

The new microfluidic format is made possible by our recently developed rapid prototyping method for digital microfluidics, which makes use of flexible, copper-clad polyimide substrates,[22] which can be bent into topographies with radii as small as 2 mm. To take full advantage of this flexibility, we used the open digital microfluidics device configuration (which has been described elsewhere[23,24]) instead of the more common enclosed configuration.[1,2,7,8] A disadvantage of this configuration is accelerated droplet evaporation; for applications in which this is a problem, evaporation can be minimized by enclosing devices in a humidified chamber.[12]

ATDA devices were formed by patterning arrays of copper electrodes and coating them with poly(dimethylsiloxane) (PDMS) and Teflon-AF. Droplets were actuated by applying potentials to sequential pairs of electrodes (Fig. 1a), enabling movement on inclined, declined, vertical, twisted, and upside-down surfaces (Fig. 1b–f). Additionally, ATDA was found to

[a]*Department of Mechanical and Industrial Engineering, University of Toronto, 5 King's College Road, Toronto, Ontario, M5S 3G8, Canada*
[b]*Department of Chemistry, University of Toronto, 80 St. George Street, Toronto, Ontario, M5S 3H6, Canada. E-mail: awheeler@chem.utoronto.ca; Fax: +1 (416) 946-3865; Tel: +1 (416) 946-3864*
[c]*Institute of Biomaterials and Biomedical Engineering, University of Toronto, 164 College Street, University of Toronto, Toronto, Ontario, M5S 3G9, Canada*
[d]*Banting and Best Department of Medical Research, University of Toronto, 112 College street, Toronto, Ontario, M5G 1L6, Canada*
† Electronic supplementary information (ESI) available: Supplementary figures and ATDA movie. See DOI: 10.1039/b801516c

 This journal is © The Royal Society of Chemistry 2008

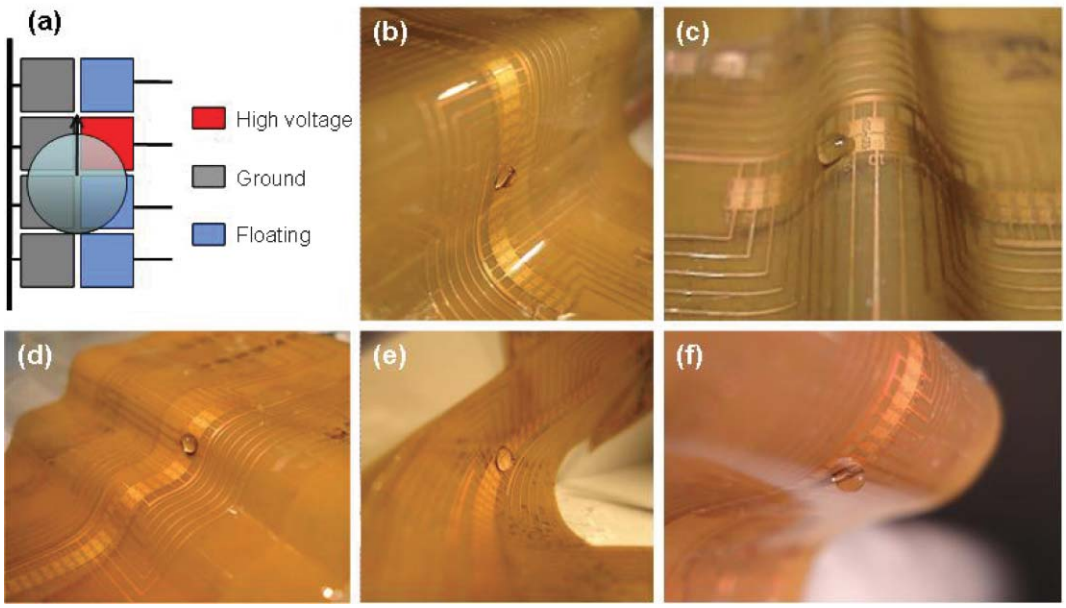

Fig. 1 ATDA manipulation of droplets. (a) Actuation scheme. (b) Droplet moving up a 15 mm high wall. (c) Droplet moving up a "bridge". (d) Droplet moving down a staircase. (e) Droplet moving on a "twist". (f) Upside-down droplet movement.

be capable of manipulating droplets through an air–oil interface (ESI Fig. S1†). In all geometries, droplet movement was facile and fast, with no significant differences relative to conventional, planar microfluidics. As is the case for standard devices,[25] ATDA was demonstrated to be capable of actuating a wide variety of liquids, including aqueous buffers, solutions of proteins and DNA, and undiluted bovine serum. A movie depicting ATDA manipulations on several kinds of structures can be found online in the ESI.†

The flexibility of ATDA substrates facilitates the formation of horizontal and non-horizontal regions on a single device. This is an important advantage, enabling a single device to be used to manipulate droplets over non-horizontal surfaces, and to passively hold droplets static on horizontal surfaces (without applying driving potentials). If a (conventional) planar device was simply tilted at an angle, a droplet could *only* be held static by non-stop application of driving potentials, which (after a few seconds) causes dielectric breakdown and device failure. Moreover, for more complex device geometries with bussed electrodes,[5,26] continuous application of driving potentials to keep a given droplet static could disturb the manipulation of other droplets. ATDA suffers from neither of these limitations.

ATDA model

Since droplets have never before been manipulated on surfaces like those shown in Fig. 1, we developed a model for predicting the parameters of droplet motion on non-horizontal substrates. The conventionally accepted mechanism for droplet actuation on horizontal devices is electrowetting-on-dielectric (EWOD), which is described in detail by Lee *et al.*[1] In such devices, there are two forces that regulate droplet motion, an actuation force, F_{EWOD}, resulting from Laplace pressures arising from the difference in the contact angles on two sides of a droplet, and a resistive friction force, F_{f}, resulting from contact angle hysteresis (*i.e.*, line pinning[27,28]) and viscous friction.[29,30] A parameter that has no effect in horizontal EWOD but must be considered in ATDA is gravity, which introduces an additional force, F_{g}, that resists droplet motion up an inclined plane. Since F_{EWOD} is limited by the maximum contact angle difference that can be achieved (which is independent of volume), whereas F_{g} is a linear function of droplet volume, there should be a maximum droplet size that can be driven up a plane at a given inclination angle.

To predict droplet movement by ATDA, we estimated F_{EWOD}, F_{f}, and F_{g} for droplet movement up an inclined plane. Since most conventional derivations of F_{EWOD}[1] arise from a different configuration than is used for ATDA, we approximated F_{EWOD} instead using the Carre and Shanahan model[31] for calculating capillary forces resulting from contact angle hysteresis:

$$F_{\mathrm{EWOD}} \approx F_{\mathrm{capillary}} \cong \frac{1}{2}\pi r_0 \gamma_{\mathrm{LV}} \left(\cos\theta_{\mathrm{adv}} - \cos\theta_{\mathrm{rec}}\right) \qquad (1)$$

where r_0 is the radius of the droplet base, γ_{LV} is the liquid–vapor surface tension, and θ_{adv} and θ_{rec} are the advancing and receding contact angles, respectively (ESI Fig. S2†). To calculate the maximum F_{EWOD}, we used the maximum electrically driven contact angle difference that can be achieved for droplets on our devices, $\theta_{\mathrm{adv}} = 68\,^{\circ}$ and $\theta_{\mathrm{rec}} = 115\,^{\circ}$ (measured experimentally). This maximum difference cannot be increased by applying higher driving potentials because of contact angle saturation.[32] To estimate F_{f}, we generated a standard curve of the resistive force acting on static droplets that prevents them from sliding down a tilted plane. Empirical data for 15 different droplet volumes were collected, and fit with a power function, as shown in the ESI Fig. S3.† We note that for droplets of the size range tested in this study, the measured static friction force (caused by line-pinning[27,28]) is more than 30 times larger than viscous friction forces[29,30] acting on moving droplets; thus, viscous friction was neglected in the model. Finally, the third force

affecting droplet movement in ATDA, F_g, was calculated simply as the projection of droplet weight down the inclined plane.

Using the forces described above, we can predict the feasibility of droplet actuation by ATDA. We note that this is a unique characteristic of the model presented here; previous descriptions of EWOD driving forces have not attempted to quantify the forces resisting movement (*i.e.*, F_f), meaning that droplet movement feasibility as a function of volume has never before been predicted. The solid line in Fig. 2 represents the largest device inclination angle at which the actuation force (for a given droplet volume) is predicted to be larger than or equal to the resistive forces.

$$F_{EWOD} \geq F_f + F_g \quad (2)$$

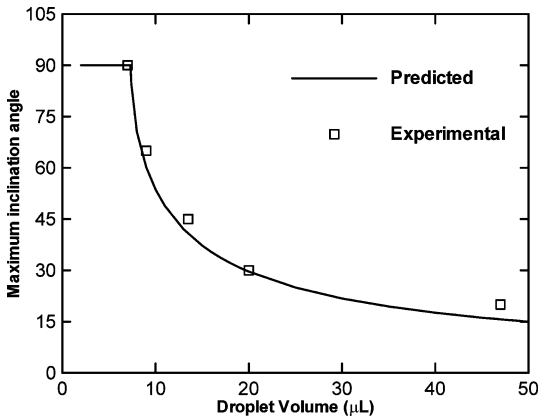

Fig. 2 Prediction and test of droplet actuation by ATDA. The solid line represents the largest inclination angles for which the model predicts successful actuation. The open boxes represent experimental observations of droplet actuation feasibility, in which ATDA was used to manipulate droplets of 7, 9, 13.5, 20, and 47 μL on 90°, 65°, 45°, 30°, and 20°, respectively. As shown, there was excellent agreement between prediction and experimental results.

As shown, this curve predicts that droplets with volumes less than ~7.3 μL can be driven up a 90 ° incline, while droplets with larger volumes can only be driven up reduced inclinations. To test this prediction, we used ATDA to manipulate droplets of different volumes and recorded the maximum inclination angle at which actuation was feasible. These data are plotted as open squares in Fig. 2; as shown, the experiments showed excellent agreement with the prediction. Note that the curve predicts that droplets of a given volume can climb any inclination up to the maximum angle specified. Thus, the further the inclination angle is below the maximum, the lower the actuation force (and the lower the applied potential) needed to drive a droplet up the inclined plane.

An interesting consequence of the new model is the prediction that very large droplets can be manipulated on horizontal (or near-horizontal) substrates, as shown in Fig. 2. This is a surprising prediction, as DMF has historically been applied to actuating very small droplets (*i.e.*, ~μL or less[1,2,5–10,18,19,22–26]). To test this prediction, we formed devices with large electrodes (25 × 30 mm), which were capable of manipulating droplets with volumes as large as 2.8 mL (shown in the ESI Fig. S4†). These results are remarkable, suggesting that digital "millifluidics" may be useful for applications requiring large volumes, *e.g.*, concentration of analytes present in trace concentrations in ~mL samples for environmental analysis. Although this is interesting, large volume droplet manipulation is tangential to the focus of this work: the introduction of ATDA as a mode of fluid transport.

ATDA applications

ATDA makes the process of integrating distinct physicochemical environments on a single, monolithic device very straightforward in comparison to the alternatives, which typically require significant microfabrication (*e.g.*, patterning resistive heating structures in lab-on-a-chip devices for PCR[7]). To illustrate this principle qualitatively, we developed methods relying on ATDA to cycle droplets between distinct (a) temperature or (b) oxygen milieus. The former is shown in Fig. 3a—a droplet containing a thermo-responsive dye (black < 29°C < white) can sample multiple thermal conditions simply by driving it onto an air-cooled open structure (where the droplet is colored black) or down to a warm hot plate (where the droplet is colored white).

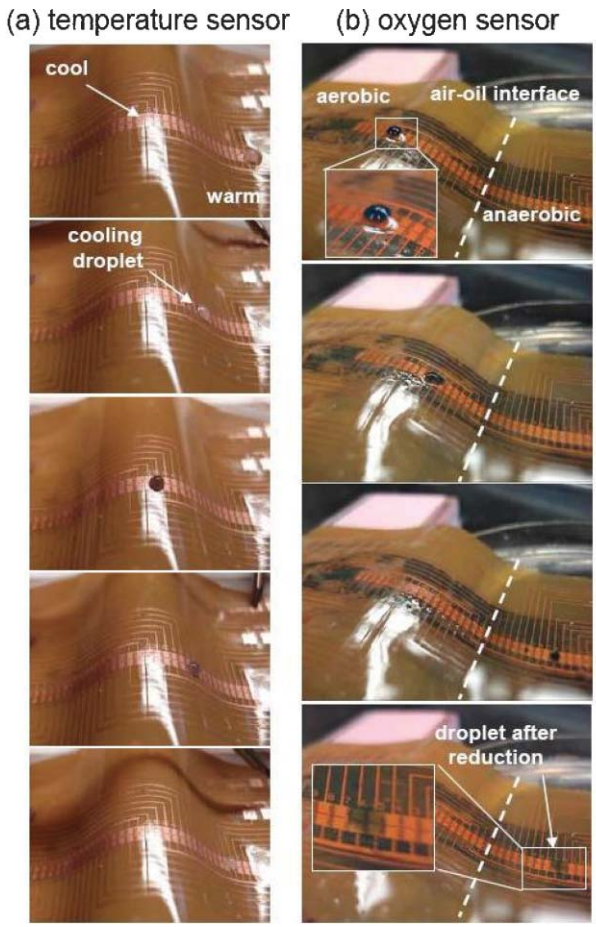

Fig. 3 Sequences of frames from movies (top to bottom) depicting multi-environmental ATDA devices. (a) Droplet containing thermo-responsive dye (black < 29°C < white) is driven up and down an air-cooled structure on a device positioned on a hot-plate held at 40°C. (b) Droplet containing methylene blue dye and glucose is driven from an aerobic chamber to an anaerobic chamber (submerged in silicone oil). In anaerobic conditions, the dye is reduced and the droplet becomes colorless.

This journal is © The Royal Society of Chemistry 2008

In the work presented here, actuation potentials were applied manually, limiting the overall droplet movement to relatively slow velocities. However, the droplet velocity between electrodes was in the range of centimeters per second, which is consistent with what has been reported previously.[33,34] We predict that in future devices driven by an automated switching box, ATDA will be capable of translating droplets very rapidly between different temperatures, suggesting utility for PCR or other applications requiring rapid temperature cycling.[7,21]

A qualitative colorimetric oxygen sensor is shown in Fig. 3b—in this geometry, an ATDA device is partially submerged in a chamber containing water-immiscible oil. When a droplet containing methylene blue dye is exposed to an aerobic environment, it remains colored blue (*i.e.*, the dye is oxidized), and when driven into an anaerobic chamber (submersed in oil), the dye is reduced and the droplet is colorless. This application relies on the capacity to drive droplets across an air–oil interface (ESI Fig. S1†). We note that this phenomenon (crossing air–oil interfaces) has been demonstrated for other lab-on-a-chip geometries;[35] however, it is exceptionally straightforward to implement in ATDA, requiring simply that a device be partially immersed in an anaerobic chamber. As this phenomenon is rapid and reversible, ATDA may prove to be useful for implementing biofuel cells or other applications that require cycling reagents between aerobic and anaerobic conditions.[36]

The most promising application that we have developed for ATDA is an automated method for enrichment of oligonucleotides from a solution containing histones. This is a standard procedure in molecular biology, in which recombinant DNA in cell lysate is purified by liquid–liquid extraction (LLE) in phenolic media. This procedure is tedious and slow, which is problematic for high-throughput applications, such as analyzing lysates of each of the 5,916-member *S. cerevisiae* single-gene deletion library.[37] To automate LLE by ATDA, we used a platform similar to the one shown in Fig. 3b to drive droplets containing a 20-bp DNA analyte and histone contaminants from an open surface into a water-immiscible phenolic solution. After LLE, the droplet was driven back to the interface and collected for analysis by mass spectrometry. Fig. 4 shows representative spectra generated from control and extracted samples. As shown, in the spectrum of the control sample (Fig. 4a), no peak corresponding to oligonucleotide is observed, presumably because of ion suppression by the high concentration of histones. In the spectrum of the extracted sample (Fig. 4b), a peak at m/z 1534 is observed, representing the $[M + 4H]^{4+}$ ion of the oligonucleotide. We speculate that future generations of ATDA devices capable of multiplexed, automated LLE, could facilitate efficient use of molecular barcode arrays (*i.e.*, distinct 20-bp DNA tags) in single-gene deletion libraries of *S. cerevisiae*.[38]

Conclusion

In conclusion, ATDA represents a new format for microfluidics, in which discrete droplets are actuated on non-planar surfaces in diverse geometries. The new technique was used to form colorimetric temperature- and oxygen-sensors, as well as to perform liquid–liquid extraction to enrich oligonucleotides from a solution containing proteins. We speculate that ATDA will be useful for a variety of applications that require cycling samples and reagents between distinct reaction conditions, such as PCR, recombinant synthesis, or industrial biocatalysis.

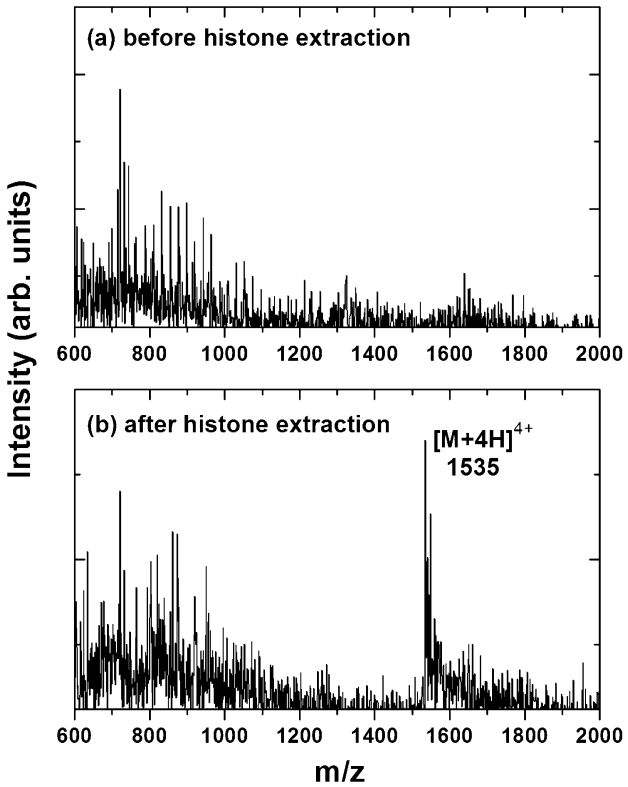

Fig. 4 Mass spectra of samples containing DNA and histones. (a) Spectrum of non-processed (control) sample. (b) Spectrum of sample enriched by ATDA-driven liquid–liquid extraction in phenol.

Methods

Device fabrication and operation. Flexible electrode arrays for ATDA devices were fabricated as described previously.[22] Briefly, arrays of 1 ×1 mm electrodes separated by 60 μm were formed by patterning flexible PCB substrates (9 μm copper on 50 μm polyimide film) from DuPont Electronic Materials (AP7156E, Research Triangle Park, NC) using photolithography and wet etching. A 9 μm thick dielectric layer and 50 nm thick hydrophobic layer were deposited by spin-coating poly(dimethylsiloxane) (PDMS) (6000 rpm, 1 min) and Teflon-AF1600 (1% resin in Fluorinert FC-40, 2000 rpm, 1 min), respectively. Devices were shaped by hand, and 1.5–7.5 μL droplets were actuated by applying AC potentials (18 kHz, 500–700 V_{RMS}, depending on geometry) between electrode pairs, as depicted in Fig. 1a. A thin film of silicone oil (DMS-TO1, Gelest Inc., Morrisville, PA) was applied to the surface when actuating biological fluids (*e.g.* proteins, serum and DNA) to reduce non-specific adsorption and enhance droplet motion; if silicone oil is not desired, a similar effect can be achieved using pluronic additives.[39]

While most ATDA devices were formed from flexible substrates, in the experiments used to generate the curve in Fig. 2, which required precise control of device inclination, we used non-flexible test substrates and devices. Test substrates were simply glass slides covered with 50 nm Teflon-AF by spin-coating, as above, and non-flexible devices had arrays of

chromium electrodes patterned by photolithography and wet etching, and were coated with 4 μm parylene and Teflon-AF (spin-coated as above).

ATDA model. A prediction of droplet motion in ATDA was generated relying on F_{EWOD}, F_f, and F_g. Modeling F_{EWOD} was straightforward—the driving force as a function of volume is given by eqn (1), with $r_0 = \left(3V\sin^3(\theta)/\pi\left[2-3\cos(\theta)+\cos^3(\theta)\right]\right)^{1/3}$, where radius r_0 is in m, volume V is in m^3 and static contact angle $\theta = 115$ °, $\gamma_{LV} = 0.072$ N m^{-1}, $\theta_{adv} = 68$ °, and $\theta_{rec} = 115$°. Modeling F_f required fitting to empirical data, which were generated by pipetting droplets of DI water onto test substrates, and tilting the surfaces until the droplets were observed to slide. The inclination angle causing each droplet to slide was recorded and the friction force as a function of volume was estimated as the projection of the droplet weight along the measured inclination angle. For each volume, 3–5 droplets were evaluated to find the average sliding angle and thus the average static friction force. As shown in the ESI Fig. S3†, forces for 15 different droplet volumes were fit to a power function to estimate the friction force, $F_f = e^{(0.40841\ln V + 0.4153)}$, where F_f is in dynes and V is the droplet volume in microliters. Finally, the third force, F_g was calculated simply as the projection of a droplet's weight along an inclined surface (note that F_g in this context is for a droplet being manipulated by ATDA, rather than the static droplets used to calculate F_f). Using the curves for F_{EWOD}, F_f, and F_g, eqn (2) was applied to generate a prediction of droplet actuation feasibility, shown as a solid line in Fig. 2.

ATDA model performance. To test the predictive value of the ATDA model, experimental measurements were performed to evaluate the maximum droplet volumes that could be driven up five different inclination angles: 90°, 65°, 45°, 30°, and 20°. For each measurement, a droplet of DI water was pipetted onto a rigid device and driven up the incline (with maximum applied potential sufficient for contact angle saturation[32]) over at least 4 pairs of electrodes. After each successful movement, a new droplet, 0.5 μL bigger than the previous one, was tested for actuation feasibility. This was repeated until the driving force was no longer sufficient for the droplet to move up the incline. This final droplet volume, less 0.5 μL, was deemed the maximum volume that could be actuated. After each initial maximum volume was recorded, at least two additional trials were carried out to confirm the initial results; in all cases, there was perfect agreement between repetitive trials (to the nearest 0.5 μL). The maximum moveable volumes for each of the tested inclination angles were plotted on Fig. 2 as open squares.

ATDA temperature and oxygen sensors. Temperature sensor devices were formed by positioning a 5 mm-tall "bridge" device on the surface of a 40 °C hotplate. A 2 μL droplet containing black leuco dye (LD-S-29C, Color Change Corporation, Streamwood, IL) diluted in DI water (1 : 100 by weight) was transported up and down the bridge by ATDA. When close to the hot surface, the droplet was white; when on the cooler bridge top, the droplet was black. The color change took place in ~12 s under these conditions. Oxygen sensor devices were formed by positioning a 7 mm-tall "step" structure in a dish such that the bottom surface was submerged in silicone oil (DMS-TO1, Gelest Inc., Morrisville, PA), and the top surface was exposed to air. A 2 μL droplet containing methylene blue dye and other reagents (0.01% dye, 10 mg mL^{-1} glucose, and 10 mg mL^{-1} NaOH in DI water) was colored blue when exposed to air, but became clear when driven into the oil. Nitrogen was bubbled through oil prior to use to displace any dissolved oxygen. For both sensors, the droplets could be actuated between the environmental conditions repeatedly.

ATDA DNA enrichment. Aqueous stock solutions of calf muscle type IIA histone and 20-mer pre-desalted DNA oligonucleotide (5′AGCAGAGCGACCTCAATGAT3′) (Sigma Aldrich, Oakville, ON) were formed by dissolving them individually in DI water. A working solution was prepared (2.5 μM DNA, 25 μg mL^{-1} protein), and a 2 μL droplet was pipetted onto a device similar to the one shown in Fig. 3b. The droplet was driven into a solution of phenol (2.5% by weight in DMS-TO1 silicone oil), and then cycled on submerged electrodes for around 1 min before being driven back to the air–oil interface. The processed droplet and an equal volume of non-processed (control) solution were diluted separately into 40 μL of water–methanol (50% vol/vol) for analysis. Samples were injected into an LTQ linear ion trap mass spectrometer in positive ion mode (Thermo Fischer Scientific, Waltham, MA). Samples were delivered *via* a fused silica-capillary transfer line (100 μm id) mated to a nanoelectrospray emitter tip (30 μm id) at a flow rate within the range of 0.5–1 μL min^{-1}, with an applied voltage within the range of 1.7–1.9 kV and capillary temperature of 170 °C. The data shown in Fig. 4 represents an average of 10 acquisitions, and are representative of multiple samples analyzed. The peak at m/z 1535 (also observed in spectra of samples containing only DNA, not shown) represents the $[M + 4H]^{4+}$ oligonucleotide, where M is the parent molecule (MW= 6135).

Acknowledgements

We thank Deborah Zamble, Sheila Wang, and Rebecca Jockusch for helpful discussions. We thank the Natural Sciences and Engineering Council (NSERC) and the Canada Foundation for Innovation (CFI) for financial support. M. Abdelgawad thanks the OGS program for an Ontario Graduate Scholarship. ARW thanks the CRC for a Canada Research Chair.

References

1 J. Lee, H. Moon, J. Fowler, T. Schoellhammer and C.-J. Kim, *Sens. Actuators, A*, 2002, **95**, 259–268.
2 M. G. Pollack, R. B. Fair and A. D. Shenderov, *Appl. Phys. Lett.*, 2000, **77**, 1725–1726.
3 M. Washizu, *IEEE Trans. Ind. Appl.*, 1998, **34**, 732–737.
4 O. D. Velev, B. G. Prevo and K. H. Bhatt, *Nature*, 2003, **426**, 515–516.
5 V. Srinivasan, V. K. Pamula and R. B. Fair, *Lab Chip*, 2004, **4**, 310–315.
6 T. Taniguchi, T. Torii and T. Higuchi, *Lab Chip*, 2002, **2**, 19–23.
7 Y.-H. Chang, G.-B. Lee, F.-C. Huang, Y.-Y. Chen and J.-L. Lin, *Biomed. Microdev.*, 2006, **8**, 215–225.
8 A. R. Wheeler, C. A. Bird, J. A. Loo, R. L. Garrell, R. R. O. Loo, C. J. Kim and H. Moon, *Anal. Chem.*, 2005, **77**, 534–540.
9 A. R. Wheeler, H. Moon, C. J. Kim, J. A. Loo and R. L. Garrell, *Anal. Chem.*, 2004, **76**, 4833–4838.
10 H. Moon, A. R. Wheeler, R. L. Garrell, J. A. Loo and C. J. Kim, *Lab Chip*, 2006, **6**, 1213–1219.

 This journal is © The Royal Society of Chemistry 2008

11 E. M. Miller and A. R. Wheeler, *Anal. Chem.*, 2008, **80**, 1614–1619.
12 I. Barbulovic-Nad, H. Yang, P. S. Park and A. R. Wheeler, *Lab Chip*, 2008, **8**, 519–526.
13 H. Wu, T. W. Odom, D. T. Chiu and G. M. Whitesides, *J. Am. Chem. Soc.*, 2003, **125**, 554–559.
14 G. Mensing, T. Pearce and D. J. Beebe, *J. Assoc. Lab. Autom.*, 2005, **10**, 24–28.
15 T. Thorsen, S. J. Maerkl and S. R. Quake, *Science*, 2002, **298**, 580–584.
16 Y. Kikutani, H. Hisamoto, M. Tokeshi and T. Kitamori, *Lab Chip*, 2004, **4**, 328–332.
17 Y. Kikutani, T. Horiuchi, K. Uchiyama, H. Hisamoto, M. Tokeshi and T. Kitamori, *Lab Chip*, 2002, **2**, 188–192.
18 H. Yang, S.-K. Fan, C.-P. Lin, C.-T. Wu and W. Hsu, in *Proceedings of 2005 ASME International Mechanical Engineering Congress and Exposition*, ASME, Three Park Avenue, New York, 2005, p. 80744.
19 J.-M. Roux, Y. Fouillet and J.-L. Achard, *Sens. Actuators, A*, 2006, **134**, 486–493.
20 R. D. Schaeffer and G. Kardos, *Printed Circuit Des. Manuf.*, 2006, **23**, 38–42.
21 K. Shen, X. Chen, M. Guo and J. Cheng, *Sens. Actuators, B*, 2005, **105**, 251–258.
22 M. Abdelgawad and A. R. Wheeler, *Adv. Mater.*, 2007, **19**, 133–137.
23 C. Cooney, C.-Y. Chen, M. Emerling, A. Nadim and J. Sterling, *Microfluidics Nanofluidics*, 2006, **2**, 435–446.
24 U.-C. Yi and C.-J. Kim, *J. Micromech. Microeng.*, 2006, **16**, 2053–2059.
25 D. Chatterjee, B. Hetayothin, A. R. Wheeler, D. J. King and R. L. Garrell, *Lab Chip*, 2006, **6**, 199–206.
26 R. B. Fair, *Microfluidics Nanofluidics*, 2007, **3**, 245–281.
27 J. Berthier, P. Dubois, P. Clementz, P. Claustre, C. Peponnet and Y. Fouillet, *Sens. Actuators, A*, 2007, **134**, 471–479.
28 S. W. Walker and B. Shapiro, *J. MEMS*, 2006, **15**, 986–1000.
29 R. S. Subramanian, N. Moumen and J. B. McLaughlin, *Langmuir*, 2005, **21**, 11844–11849.
30 F. Brochard, *Langmuir*, 1989, **5**, 432–438.
31 A. Carre and M. E. R. Shanahan, *J. Adhes.*, 1995, **49**, 177–185.
32 H. Moon, S. K. Cho, R. L. Garrell and C. J. Kim, *J. Appl. Phys.*, 2002, **92**, 4080–4087.
33 S. K. Cho, H. Moon and C. J. Kim, *J. MEMS*, 2003, **12**, 70–80.
34 M. G. Pollack, R. B. Fair and A. D. Shenderov, *Lab Chip*, 2002, **2**, 96–101.
35 R. B. Fair, A. Khlystov, V. Srinivasan, V. K. Pamula and K. N. Weaver, in *Proceedings of the International Society for Optical Engineering*, ed. L. A. Smith and D. Sobek, SPIE, Bellingham, Wash, 2004, vol. 5591, pp. 113–124.
36 S. K. Chaudhuri and D. R. Lovley, *Nat. Biotechnol.*, 2003, **21**, 1229–1232.
37 G. Giaever *et al.*, *Nature*, 2002, **418**, 387–391.
38 S. E. Pierce, E. L. Fung, D. F. Jaramillo, A. M. Chu, R. W. Davis, C. Nislow and G. Giaever, *Nat. Methods*, 2006, **3**, 601–603.
39 V. N. Luk, G. C. Mo and A. R. Wheeler, *Langmuir*, 2008, DOI: 10.1021/la7039509.